

# A Computational Fluid Dynamics Model for Drug Delivery in a Nasal Cavity with Inferior Turbinate Hypertrophy

Xiao Bing Chen, Ph.D.,<sup>1</sup> Heow Pueh Lee, M.S., Ph.D.,<sup>1</sup> Vincent Fook Hin Chong, M.D.,<sup>2</sup>  
and De Yun Wang, M.D., Ph.D.<sup>3</sup>

## Abstract

**Background:** Intranasal medications are commonly used in treating nasal diseases. However, technical details of the correct usage of these medications for nasal cavity with obstruction are unclear.

**Methods:** A three-dimensional model of nasal cavity was constructed from MRI scans of a healthy human subject. Nasal cavities corresponding to healthy, moderate, and severe nasal obstruction (NO) were simulated by enlarging the inferior turbinate geometrically, which was documented by approximately one-third reduction of the minimum cross-sectional area for the moderate and two-thirds for the severe obstruction. The discrete phase model based on steady-state computational fluid dynamics was used to study the gas–particle flow. The results were presented with drug particle (from  $7 \times 10^{-5}$  to  $10^{-7}$  m) deposition distribution along the lateral walls inside these three nasal cavities, and comparisons of the particle ratio escaping from the cavity were also presented and discussed.

**Results:** Nasal patency is an essential condition that had the most impact on particle deposition of the factors studied; the particle percentage escaping the nasal cavity decreased to less than a half and one-tenth for the moderately and severely blocked noses. Decreasing of flow rate and particle diameter increased the escaping ratio; however, zero escaping percentage was detected with the absence of air flow and the effect was less noticeable when the particle diameter was very small ( $<10^{-6}$  m). The existence of inspiratory flow and head tilt angle helped to improve the particle escaping ratio for the healthy nose; however, such changes were not significant for the moderately and severely blocked noses.

**Conclusion:** When using an intranasal medication, it is advisable to have a moderate inspiratory air-flow rate and small size particles to improve particle escaping ratio. Various head positions suggested by clinicians do not seem to improve the drug escaping ratio significantly for the nasal cavities with inferior turbinate hypertrophy.

**Key words:** drug delivery, inferior turbinate hypertrophy, computational fluid dynamics (CFD), nasal air flow, particle deposition

## Introduction

A LARGE NUMBER OF INTRANASAL MEDICATIONS such as intranasal corticosteroids (INS) are being used as the standard treatment for patients suffering from allergic rhinitis and rhinosinusitis, which appear to be the most prevalent airway diseases worldwide.<sup>(1,2)</sup> In addition to the pharmacological properties of INSs, correct usage of INS by patients is necessary to achieve optimal efficacy of the drug.

Certain practical indicators for the appropriate application of INS such as the head position and necessity of having an apnea or inspiratory flow during spray of INS are still not clear or known to both physicians and patients. In addition, nasal obstruction is a cardinal symptom of allergic rhinitis and rhinosinusitis, which is commonly seen by edema and congestion of the nasal mucosa and inferior turbinates. The impact of nasal obstruction on drug delivery and deposition, which eventually affects the efficacy of INS, is also unknown. These problems are mainly due to limitations associated with

<sup>1</sup>Department of Mechanical Engineering, <sup>2</sup>Department of Diagnostic Radiology, and <sup>3</sup>Department of Otolaryngology, Yong Loo Lin School of Medicine, National University of Singapore, Singapore.

the available techniques that are being carried out during *in vivo* human studies.

According to the reported studies, the research techniques that can be used for *in vivo* human studies to monitor drug deposition in the nose are CT imaging,<sup>(3)</sup> gamma scintigraphy,<sup>(4,5)</sup> of radio enhanced particles, or endoscopic video imaging of dyed test formulations.<sup>(6,7)</sup> These techniques are invasive or difficult to implement in human studies, and could cause exposure to radiation or lung deposition of foreign particles. In addition, the need to decongest the nose to perform endoscopic examinations is a pitfall because the operation results may not be general and cannot extrapolate to patients with rhinosinusitis. However, that is very difficult to avoid for minimized confounding effect and correct deposition of the particles.<sup>(4)</sup>

In the past decades, there have been several developments in the field of computational fluid dynamics (CFD) that enable the researchers to study nasal perforations,<sup>(8)</sup> turbinate surgery,<sup>(9,10)</sup> odorant delivery,<sup>(11)</sup> and many other general studies involving air flow in nasal cavities.<sup>(12–14)</sup> Particle drug delivery and deposition were also numerically simulated for a healthy nose cavity,<sup>(15–17)</sup> which presented the effects of particle size, diameter of spray cone, and spray cone angle on the deposition distributions on the cavity wall. However, such a numerical deposition procedure has not been implemented for a nasal cavity with turbinate hypertrophy before.

The major advantage of the CFD technique is that various types of nose models can be constructed by mimicking dif-

ferent degrees of nasal obstruction and other structural malformations. The flexibility to rapidly manipulate the geometry on the computer enables us to perform CFD analysis of the nasal air-flow pattern in normal and pathological conditions, as well as their impact on the drug deposition, when using a commercial nasal spray.

Hence, the aim of this study was to provide qualitative and quantitative information to both physicians and patients on the correct usage of intranasal medications, when treating common nasal diseases that cause inferior turbinate hypertrophy. Computational fluid dynamics tools were used to simulate the flow and drug deposition procedure inside the nasal cavity, which was constructed using a MRI scan for a healthy nose and implementing inferior turbinate expansion for moderately and severely blocked noses.<sup>(18)</sup> The results were presented with drug particle deposition distribution along the nasal walls inside these three nasal cavities and comparisons of the particle ratio escaping from the nasal cavity were also presented and discussed.

## Materials and Methods

### *Development of a healthy nose model from MRI scans*

The nasal airway geometry (Fig. 1) was constructed from a magnetic resonance imaging (MRI) scan of a healthy human subject, who was selected based on medical history, endoscopic nasal examination, and measurements of active rhinomanometry and acoustic rhinometry. The results of these assessments were within the normal range of our previous

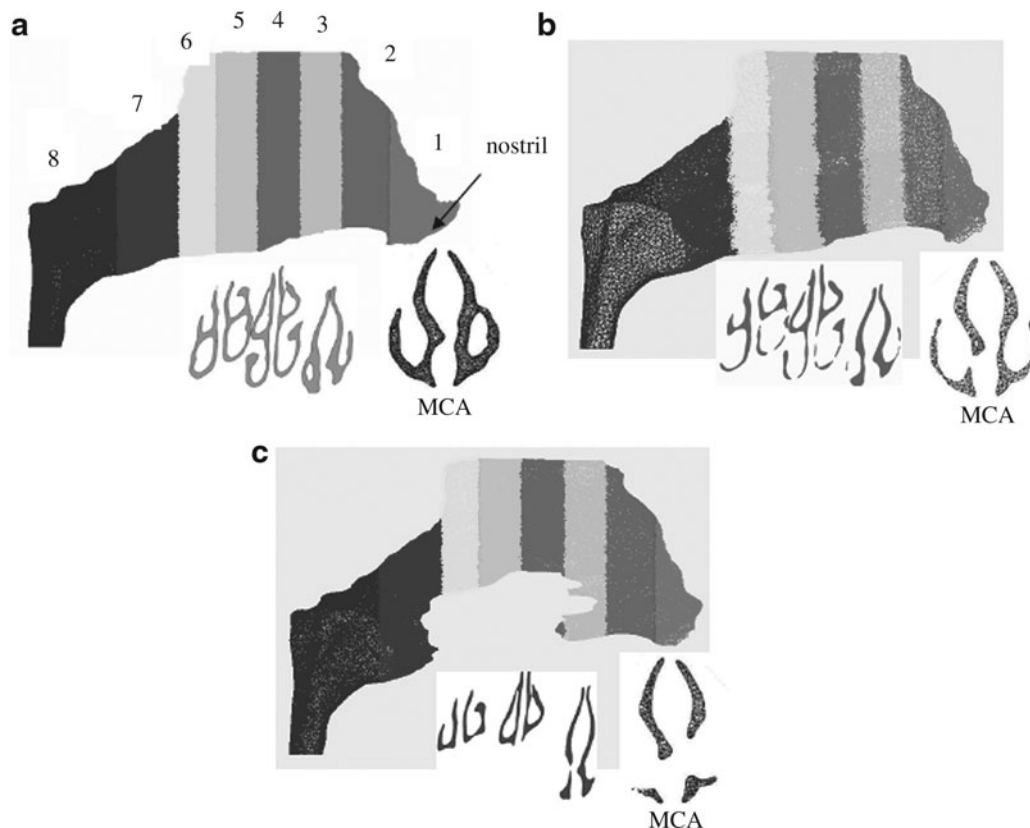


**FIG. 1.** Different sections (from right to left section 1–8), coronal cross sections and MCA of the nasal cavity for the 3-day nose models: (a) healthy nose, (b) moderately blocked nose, (c) severely blocked nose.

studies.<sup>(19–21)</sup> The scan images appeared at an interval of 1.5 mm along the vertical direction. A segmentation was performed using Mimics version 12.1 (Materialise Group, Leuven, Belgium) (<http://www.materialise.com/>) and the detailed procedures can be found in our previous reported study.<sup>(18)</sup> The main passageway comprising components such as inferior, middle, and superior meatus, and nasopharynx, were properly captured in the three-dimensional model. Thereafter, a high-resolution 3D volume mesh comprising computational domain in the nasal cavity, as well as a surrounding air volume extending 10 cm outside the nostril (Fig. 2), was constructed. The extended air volume was to enable a more realistic implementation of external boundary condition of atmospheric pressure in front of the nostrils. It is noted that the dorsal region looks rectangular in shape (Fig. 1), which is due to the corrugation shape modification (smoothing over those slightly wall ups and downs, or sudden small hollows due to segmentation error) to help decrease computational effort. The flow pattern results in our recent articles<sup>(18,22)</sup> show that few streamlines go directly to the dorsal parts, which are close to the maxillary sinus region. Numerical result comparisons show that such slight shape modifications at these regions do not affect the main flow patterns significantly inside the main internal nasal cavity.

A preliminary healthy model composed of 1 million 3D tetrahedral elements was used for average cross-section velocity profiles along the cavity wall toward the nasopharynx (Fig. 3). Two more cases (2 and 3 millions) were then constructed with the same boundary conditions for comparison, which showed some changes (maximum 9.59% differences) in the velocity profiles from 1 to 2 million cell models and the refined model consisting of 3 million cells showed no further significant improvements (maximum 1.21% differences). Similar grid convergence concerning particle deposition was also obtained with the same procedure. Thus, a typical computational model comprising about 2 million cells was adequate to ensure insensitivity to mesh density. This mesh was generated by a combination of several commercially available preprocessing software packages, including Mimics

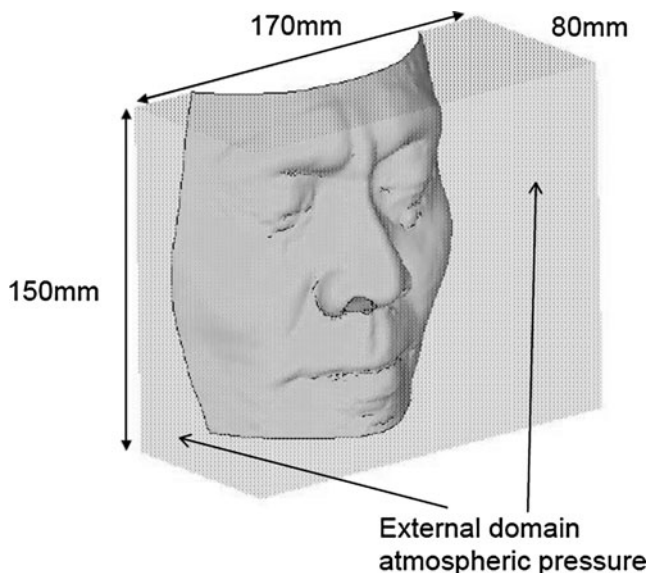


FIG. 2. Computational domain outside the nostril.

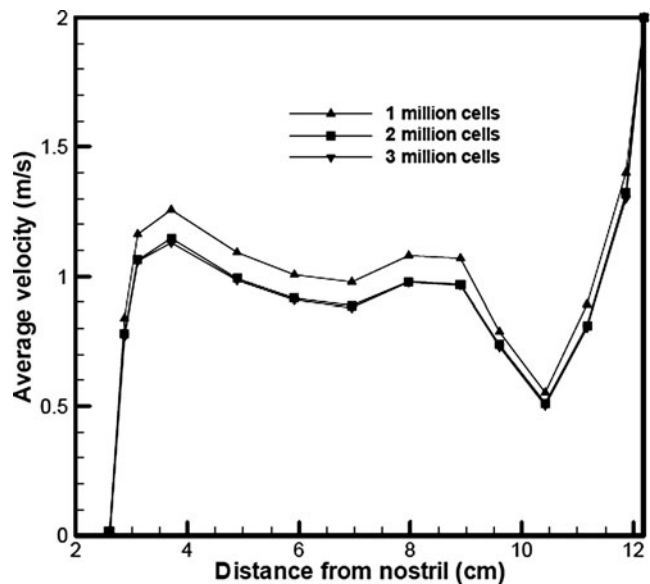


FIG. 3. Grid independent survey for the average cross-section velocity along the nasal cavity from the nostril with a nose flow rate = 17.4 L/min.

12.1, Hypermesh 9.0 (Altair Engineering, Inc., Bingham Farms, MI, USA) and TGrid 4.0 (ANSYS, Inc, Canonsburg, PA, USA).

#### Construction of diseased nose models from the healthy nose model

The software Mimics was used to “mimic” different medical conditions of the nasal cavity using morphological tools provided in the software. An in-house code was developed for arbitrary shape modification to the inferior turbinate. Basically, the rod-like inferior turbinate was expanded such that the ratio of expansion in axial and radial directions is 2:1. This deformation was performed with the advice of an ENT doctor, in such a manner that the whole inferior turbinate was enlarged normally outward by about 1 and 2 mm for simulating moderate and severe nasal obstruction, respectively. During the expansion process, whenever the inferior turbinate surface touched the opposite wall, both surfaces would be considered as collapsing and impermeable to the air flow. Thus, various degrees of severity of nasal obstruction were modeled, following which the major site of nasal resistance, namely, the minimum cross-sectional area (MCA), was identified for studying the drug penetration patterns, as this location is within the critical nasal valve (NV) region.<sup>(23)</sup> The MCA from the front end of nostril was found to be a cut plane located at 2.35 cm along the air-flow direction (e.g., perpendicular to the bulk flow direction). This location agreed with the results obtained from acoustic rhinometric (a SRE 2100 acoustic rhinometer, Rhinometrics A/S, Lyngø, Denmark) measurement<sup>(19)</sup> from the same person. This cut plane would also ensure that the plane for the MCA would intercept the front part of the inferior turbinate, so that any subsequent inferior turbinate expansion mimicking nasal obstruction would result in the reduction of the MCA.

Turbinate expansion was performed in such a manner that the whole inferior turbinate was enlarged homogeneously outward by about 1 and 2 mm for moderate and severe obstruction, respectively.<sup>(18)</sup> These classifications can be documented by approximately one-third reduction of the MCA (1.453 cm<sup>2</sup> in the healthy nose) for the moderate (0.873 cm<sup>2</sup>) and two-thirds (0.527 cm<sup>2</sup>) for the severe obstruction (Fig. 1). The ratio of MCA reduction in moderate and severe obstruction is similar to a previous study of nasal obstruction after nasal allergen challenge in patients with allergic rhinitis.<sup>(19)</sup>

#### Numerical simulation of the inspiratory air-flow field

For the computational fluid dynamic simulations, the flow was assumed to be incompressible and quasi-steady. To account for the possible existence of turbulence, the Reynolds averaged Navier-Stokes equation was solved with a  $k-\omega$  model. The  $k-\omega$  model approximation is sufficient to depict the low levels of swirling in nasal cavity,<sup>(24,25)</sup> with affordable computational effort and ability to predict pressure drop, velocity, and shear stress distributions. It is appropriate for current internal laminar, transitional, and fully turbulent flow mainly through the correction of the turbulent viscosity, its acceptable handling of shear flows, and its ability to predict the attached boundary layers in adverse pressure gradient (at expansion in flow). The shear stress transport (SST) option with transitional flow treatment was implemented to capture such complex laminar-transitional-turbulent flow. The SST model blends the  $k-\omega$  (applied near wall) and  $k-\varepsilon$  turbulent models (applied at the main flow domain), which is ideal for flow in complex geometry such as the nasal cavity.<sup>(24)</sup> The turbulence intensity was set to 6% and the dissipation rate was set at a dissipation length scale of 0.1 cm at the inlet and outlet boundaries. A constant flow rate of 8.7, 17.4, 34.8, and 52.2 L/min at the nasopharynx area was applied as the boundary condition. The increased flow rate was used to model different breathing status (e.g., calm inspiration, middle and strong sniffing)<sup>(15,17,18,26)</sup>. At the external enclosure of the face (Fig. 2), the pressure inlet boundary condition was applied with gauge pressure equal to zero (atmospheric pressure). For the particles, the effects of accretion and erosion were not considered, and particles were assumed to be trapped once they hit the cavity wall.

#### Numerical modeling of the drug/particle motion in the computed air-flow field

The discrete phase model (DPM) was used to study the gas-particle flow (Fig. 4). The Euler-Lagrange approach was implemented by the Lagrangian DPM in Fluent 6.3 package (ANSYS, Inc.) (<http://www.fluent.com/>). It made use of a Lagrangian particle tracking method accompanied by discrete random walk technology for turbulent dispersion of particles. The confirmation of DPM module in the CFD software Fluent for its accuracy, efficiency, and consistency for drug particle deposition inside the nasal cavities and its detailed acceptable assumptions and mathematical equations can be found in previous studies.<sup>(16,26,27)</sup> The agreement in Figure 5 for the comparison of the deposition efficiency with the previous published experimental results<sup>(28-30)</sup> in a healthy nasal cavity suggested that the current nasal cavity model could be used for realistic particle deposition simulations.

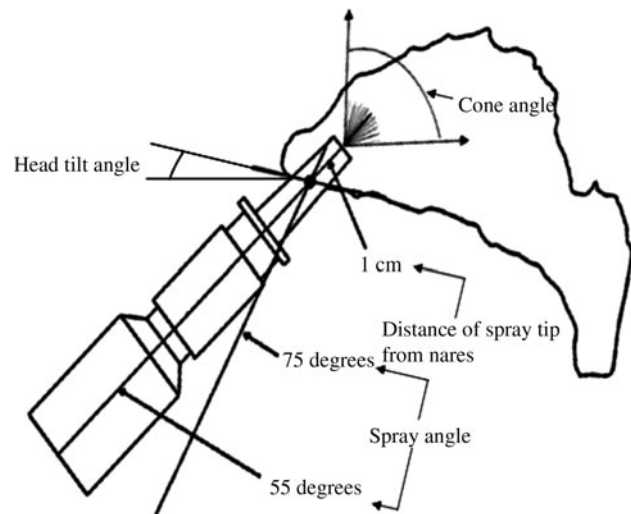


FIG. 4. Schematic descriptions of different geometric drug delivery parameters and position of nasal spray (outlines partially reproduced from Fig. 2 by Kimbell et al.<sup>(15)</sup> and currently illustrated with more proper captions).

With a passively released particle diameter around 60  $\mu\text{m}$ ,<sup>(30)</sup> zonal deposition showed that more than 95% particles were deposited in the anterior and middle nasal wall regions, which was comparable to the experimental results.<sup>(30)</sup> For detailed particle deposition in Fluent 6.1.22, recently Tian and Ahmadi<sup>(31)</sup> recommended near-wall turbulence damping corrections in the random-walk models or the usage Reynolds Stress Models. However, with the current nasal cavity model and Fluent 6.3, it was found that the results were quite similar with either of these two suggestions unless other parameters (e.g., nasal flow rate, particle diameter, particle spray velocity, etc.) were changed as shown later.

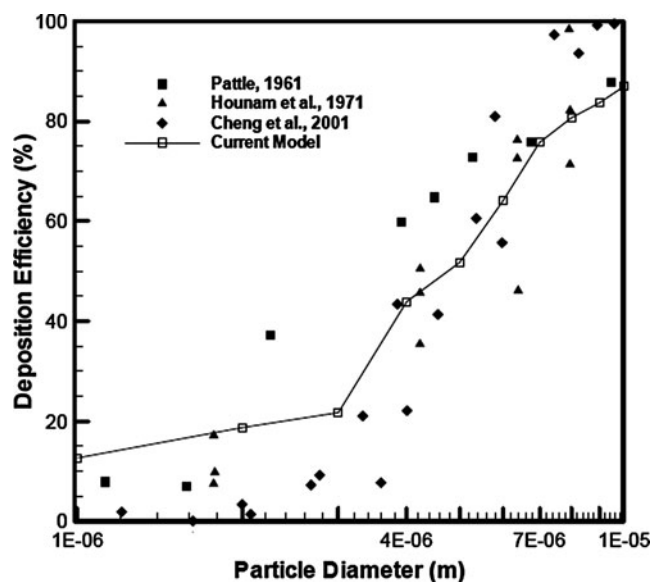


FIG. 5. Comparison of the deposition efficiency with published experimental results in the healthy nasal cavity with passively released particles; spray insertion angle = 55°, nose flow rate = 17.4 L/min, and head tilt angle = 0. (Please note a flow rate = 20 L/min was used by Cheng et al.<sup>(30)</sup>)

In the current model, the air flow was considered as a continuum when solving the conservation relationships corresponding to the steady-state Navier-Stokes equations; the dispersed phase computations were performed by tracking a large number of particles (10,000) through the air-flow field that was already solved. The particles were assumed to have a density equal to that of water ( $1000 \text{ kg/m}^3$ ) and were dispersed as a solid cone into the flow field. The trajectory of each individual discrete particle was computed at specific intervals during the dispersed phase computation that depends on the continuum computation. The particles were also assumed to be small enough that effects on flow properties were insignificant. To accurately mimic natural conditions, the impact of gravity ( $9.8 \text{ m/sec}^2$ ) was also incorporated into the numerical model.

#### *Analysis of the drug/particle deposition within different sections of the nasal cavity*

To analyze the drug/particle deposition within different sections along the cavity wall, the cavity wall was separated into eight sections from the nostril to the nasopharynx (Fig. 1a). Discrete drug particle deposition depended on particle density, particle diameter, flow rate, spray velocity, spray cone angle, spray penetration distance, spray orientation, head tilt angle, etc. In this study, these parameter values were prescribed to be the same as those values suggested by Kimbell et al.<sup>(15)</sup> Their study was based on the parameters chosen from 18 commercial nasal spray devices and 48 numerical simulation cases. In the current study, the impact of two severities of nasal blockage, compared with a normal healthy one on the drug deposition will be investigated. Moreover, the effects of initial particle velocity ( $U_s$ ), particle diameter ( $R$ ), nasal flow rate ( $Q$ ), and head tilt angle ( $\theta$ ) (as illustrated in Fig.4) will also be presented.

Particle traces inside the left nasal cavity for the healthy, moderately, and severely blocked noses were simulated with spray insertion angle  $55^\circ$ , spray cone angle  $79^\circ$ , particle density  $1000 \text{ kg/m}^3$  and spray penetration distance 1 cm from nostril as suggested by Kimbell et al.<sup>(15)</sup> These parameters remained the same when the other factors were changed for the following computations. Note that the spray device was positioned at the area-weighted centroid of each cross section corresponding to various spray distances used in this study. The centroid could be easily obtained from Fluent 6.3 package.

## **Results**

The particle traces were similar to flow streamlines in each cavity, where shifts of air flow from the ventral toward the middle and dorsal regions of the nasal passages for more severe blockage were expected.<sup>(18)</sup> Similarly, for the healthy nasal cavity (Fig. 6a), the particles mainly went around the inferior turbinate in the ventral region and for the moderately blocked nose (Fig. 6b), they changed to the upper nasal passageway around the middle turbinate in the middle region. For the severely blocked nose (Fig. 6c), particles passed closer to the superior turbinate in the dorsal region. The number of particles going through the nasal airway from the right near the nostril was found to decrease continuously due to local deposition along the cavity wall. Such a decrease of the number of particles was more apparent for the se-

verely blocked nose (Fig. 6c). For the healthy nose (Fig. 6a), due to being largest of the MCA, the particle number escaping the cavity was the largest one; for a moderately blocked nose (Fig. 6b), due to its relatively larger penetration via MCA (two-thirds left) than the severely blocked one (one-third left), the particle number escaping the cavity was larger than the severely blocked one. In Figure 6, traces were colored according to particle residence time at their specific locations. For all the three cases, the residence time was relatively longer at the nasopharynx than the initial spray position. This was because of local velocity variation, which was larger inside the cavity passageway than those regions near the nasopharynx.<sup>(18)</sup>

Moreover, the bottom views (bottom in Figures Fig. 6a, b, and c) showed that for the two blocked nasal cavities, there were more particles close to the middle septum than the cavity side wall, which showed that particles mainly deposited along the middle septum wall due to their partial passageway close to the center of the original MCA; however, for the normal healthy nose, with its complete MCA, particles were distributed relatively more uniformly along each side.

For all the three blockage cases, the largest ratio of particle deposition was located at the wall section 2; further downstream, the deposition ratio decreased, which was consistent with the reported findings by Inthavong et al.<sup>(16,26)</sup> (Fig. 7 with a constant particle size  $20 \mu\text{m}$ ). This was because the location of the minimum cross-section was between sections 2 and 3, which was measured and detailed in the previous article.<sup>(18)</sup> The MCA is the narrowest air passageway inside the nasal cavity and the main obstruction for the particle to penetrate through.<sup>(15)</sup> It can also be seen that along the wall sections 2 and 3, the deposition ratio for the severely blocked nose was the largest among the three; for further downstream wall sections, relatively smaller deposition ratio was detected. On the contrary, for the healthy nose, it was the smallest at wall sections 2 and 3, and relatively larger further downstream. These resulted in relatively larger escaping ratio for the healthy nose, and two-thirds and one-third left for moderately and severely blocked noses, respectively (Fig. 7). Thus, it could be concluded that the hypertrophy of the inferior turbinate affected particle deposition mainly through the decreasing area of the MCA.

For all the three cases, the percentage of escaping particles was higher with a flow rate  $8.7 \text{ L/min}$ ; further increasing of the flow rate decreased the escaping ratio and started to level off at a flow rate of  $17.4 \text{ L/min}$  (Fig. 8 with a constant particle size  $20 \mu\text{m}$ ). The increasing of initial particle velocity decreased the escaping ratio for the healthy nose; however, for moderately and severely blocked noses, the effect of initial particle velocity was not significantly observable.

For all the three cases, particle escaping ratio tended to decrease as the diameter of the discrete phase particles increased for all the three cases ( $>10^{-5} \text{ m}$ ) (Fig. 9 with a nose flow rate  $17.4 \text{ L/min}$ ), which was also observed with similar patterns in the previous studies.<sup>(15,16,26,32,33)</sup> However, further decreasing of particle diameter ( $<10^{-6} \text{ m}$ ) did not increase the escaping ratio furthermore. This might be due to the negligible particle inertia for small diameter particles, which made them trace the flow stream in a shorter time; and for relatively larger diameter particles (around  $10^{-5} \text{ m}$ ), the inertia effect was so large that they followed the initial

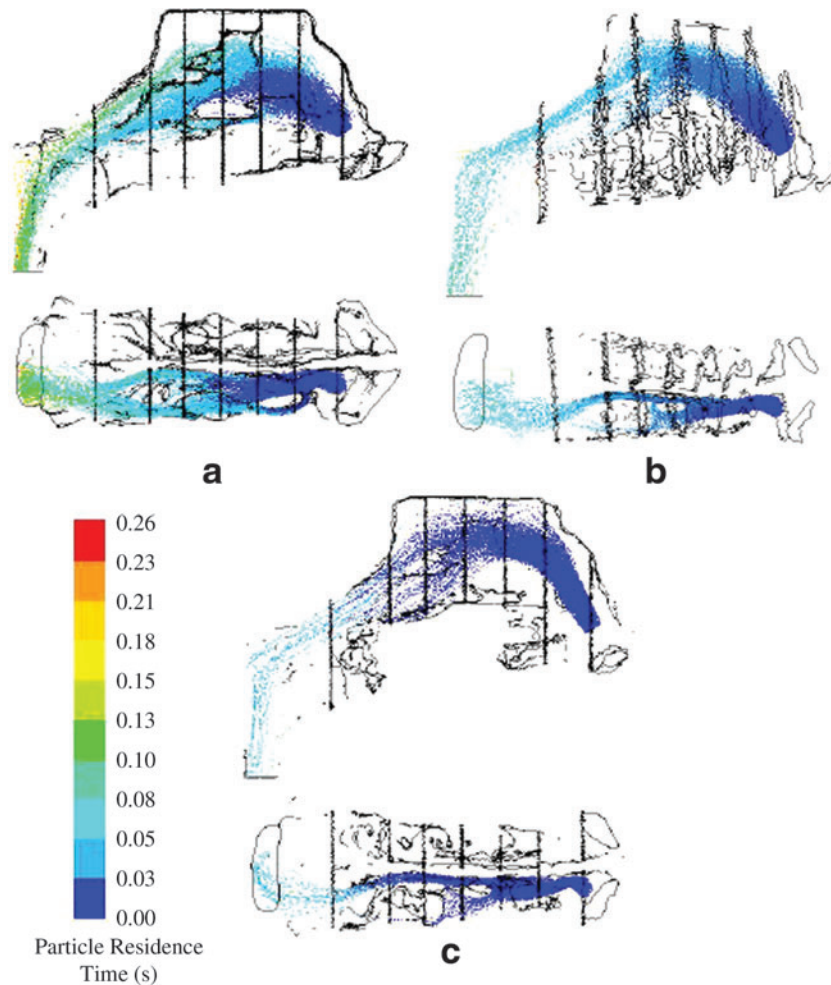


**FIG. 6.** Side and bottom views of particle traces inside the left cavity with initial particle velocity = 1 m/sec, particle diameter =  $20\ \mu\text{m}$ , spray insertion angle =  $55^\circ$ , nose flow rate = 17.4 L/min, and head tilt angle = 0: (a) healthy nose, (b) moderately blocked nose, (c) severely blocked nose.

particle speed direction to deposit mostly in the frontier wall regions (as show in Fig. 7). It should be noted that Brownian diffusion (more dominant around  $10^{-7}$  m) was omitted in current models due to the relatively larger particle diameter considered.

For the healthy nose, the particle escaping ratio was 20 times lower when the nasal spray was not accompanied by an inspiratory air flow (zero flow rate) than that of 8.7 L/min flow; however, for the moderately and severely blocked noses, the escaping ratio was zero with absence of flow (Table 1). It should be noted that there were particles that fell out of the nostril without the presence of air flow, although in current results only the escaping particles were considered. Without the air-flow rate, differences for different head tilt angles were slight; however, for a flow rate of 8.7 L/min, the particle escaping ratio for the healthy nose decreased 6.15% with different head tilt angles and for a flow rate of 17.4 L/min, it was only 0.55%. The change for the moderately and severely blocked noses was not significantly affected by the head tilt angle. The existence of flow inside could introduce drag force into the particle dynamics, which helped particles to escape. Generally, for flow around a solid body with fixed shape, the drag force is proportional to local flow

velocity (that is proportional to flow rate). When the flow rate was small (8.7 L/min), such drag force was small, which could be more prone to be affected by the gravitational force; when the flow rate was larger (17.4 L/min), the relatively bigger drag force dictated the particle motion much more than the gravitational force, thus negating the impact of variation in head tilt angle on the particle escaping. However, such force change did not affect the nasal cavities with inferior turbinate expansion, where the decreasing of MCA dominated more as presented before.

## Discussion

INs are recommended as a standard treatment in patients with allergic rhinitis and rhinosinusitis, which affect approximately 10–25% of the world population.<sup>(1,2)</sup> The advantage of intranasal administration is that high concentration of medications can be delivered directly into the nasal mucosa. It has been well established for a healthy nose model that the efficacy of drug delivery device depends on various parameters like particle density, particle diameter, nasal air-flow rate, initial particle velocity, spray cone angle, spray penetration distance, and spray orientation.<sup>(15–17, 26, 32,33)</sup>

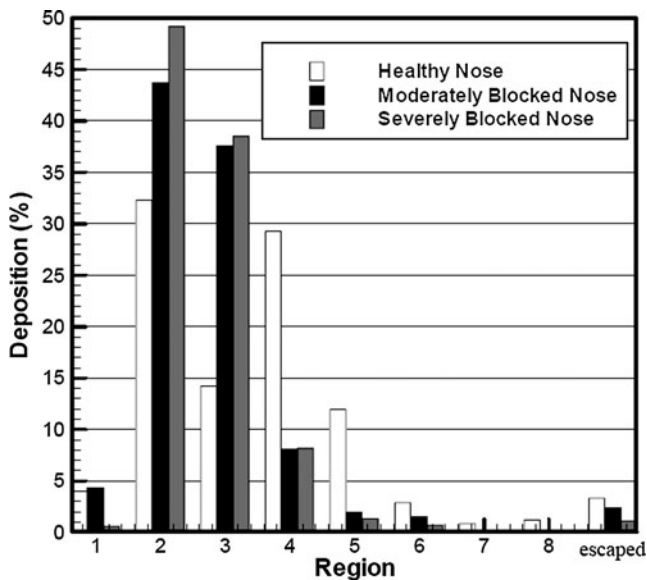


FIG. 7. Particle deposition along different sections of the nasal cavity with initial particle velocity = 1 m/sec, particle diameter = 20 μm, spray insertion angle = 55°, nose flow rate = 17.4 L/min, and head tilt angle = 0.

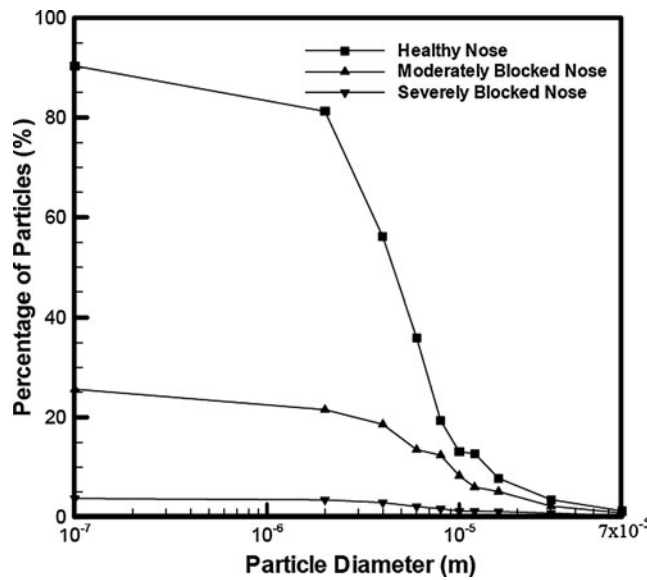


FIG. 9. Particle percentage escaping from the nasal cavity for different initial particle diameter (m) with initial particle velocity = 1 m/sec, spray insertion angle = 55°, nose flow rate = 17.4 L/min, and head tilt angle = 0.

However, the human nasal cavity has a complex structure with transient air flow and differs from each other especially for those with abnormal physiological symptoms (e.g., nasal obstruction with mucosal inflammation), which may affect the drug distribution and deposition inside. Therefore, recommendations on the usage of intranasal medications for treating nasal diseases have to account for additional considerations. Thus, the current model with two severities of nasal blockage with turbinate hypertrophy is reasonable and necessary, which may be difficult and relatively impossible

to be obtained from *in vivo* human study. This is the first attempt to investigate such deposition behavior inside the obstructed nasal passages compared with that of a normal healthy person. Although the current models are based on one specific individual and may not be representative, the current results still provides qualitative and quantitative information on the correct usage of intranasal medications for patients with inferior turbinate hypertrophy, which will contribute to the improvement of clinical efficacy of the drug/particle delivery. In the future, to make the results

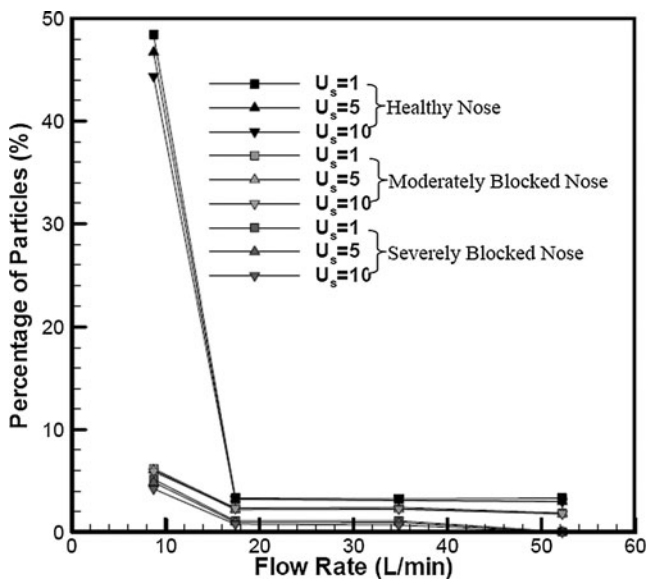


FIG. 8. Particle percentage escaping from the nasal cavity for different flow rates (L/min) and initial particle velocity  $U_s$  (m/sec) with particle diameter = 20 μm, spray insertion angle = 55°, and head tilt angle = 0.

TABLE 1. PARTICLE PERCENTAGE ESCAPING THE NASAL CAVITY IN THE PRESENCE AND ABSENCE OF INSPIRATORY FLOW WITH THE EFFECT OF HEAD TILT ANGLE AND FLOW RATE

Nasal flow rate (L/min)	Head tilt angle (degree)	Percentage for the healthy nose (%)	Percentage for the moderately blocked nose (%)	Percentage for the severely blocked nose (%)
0	0	2.07	0	0
0	30	2.15	0	0
0	60	2.08	0	0
0	90	1.68	0	0
8.7	0	48.42	6.18	5.09
8.7	30	52.01	6.54	5.14
8.7	60	46.10	5.51	5.12
8.7	90	42.27	5.36	5.06
17.4	0	3.32	2.35	1.11
17.4	30	3.87	2.43	1.14
17.4	60	3.05	1.96	1.08
17.4	90	2.96	1.95	1.06

Initial particle velocity = 1 m/sec, particle diameter = 20 μm spray insertion angle = 55°, cone angle = 79°.

generally more relevant for a patient population, a number of individual anatomies would have to be studied.

The narrowest cross-section of the nasal passage determines the nasal resistance to air flow and this area is referred to as the nasal valve (NV).<sup>(23)</sup> For a healthy nasal cavity, major changes in inspiratory air-flow pattern, with the highest velocity of air flow and wall shear stress, were found in this critical and functional region; for obstructed nasal passages, the MCA at the NV was reduced due to inferior turbinate hypertrophy, which affected local flow pattern and increased local flow velocity, shear stress and pressure loss.<sup>(18)</sup> In the current model, the particle deposition patterns changed greatly, and the differences due to inferior turbinate hypertrophy were computed. The results showed the importance of the MCA change with inferior turbinate expansion for particle deposition along the nasal cavity wall, and the presence of inspiratory air flow appeared to have a similar impact on escaping fraction. However, the other related parameters (different flow rates, initial particle velocity, particle diameter, and head tilt angles) are relatively less important for moderately and severely blocked nasal cavities (see Table 1 and Figs. 8 and 9).

Similar to previous studies of a normal healthy nose,<sup>(15,16,26)</sup> the change of flow rate and initial particle velocity do improve the particle escaping ratio for a normal healthy nose (Fig. 8). However, the results show that even with two-thirds MCA left for the moderately blocked nose, the change of flow rate and initial particle velocity together with the head tilt angle had little effect in improving the drug delivery (Fig. 8 and Table 1). Although the decreasing of particle diameter did improve more on the particle escaping ratio, there was still limited enhancement of the effect once the particle diameter is smaller than  $10^{-6}$  m (Fig. 9). The results (not presented here) showed that the effects from the changes of spray insertion angle, cone angle, and the position of the spray release point (before MCA position) were even less distinguishable for the current two obstructed nasal models, although for a normal healthy one such parameters dominate more<sup>(15,16,26,32,33)</sup>. Thus, to increase the particle escaping ratio into the lung region, for those nasal cavities with inferior turbinate hypertrophy, one possible and effective solution is to insert the spray deeper or to develop spray devices that can be inserted deeper with particles beyond the MCA region.<sup>(16)</sup> Another possible approach is a decongestive treatment to increase the MCA, which may substantially improve particle deposition along the cavity wall and increase its escaping ratio.

The results also suggest that the particle escaping ratio was larger with the presence of air flow than that with no air flow inside; however, an optimized midrange flow rate would be preferred (Table 1). Considering the results together with Figure 8, there is an optimal particle size–flow rate combination for a largest particle escaping ratio, which is consistent with the findings as Schroeter et al.<sup>(34)</sup> For low flow rate (8.7 L/min), the changing of head tilt (between 0, 30, 60, and 90 degrees) could improve the particle escaping ratio; however, when the flow rate is larger (17.4 L/min), no significant differences were found even for healthy nasal cavity. In the educational materials provided by physicians or INS producing companies, various head positions are recommended for nasal drug spray, such as head down forward position/kneeling head down, and lying head back

position. However, in practice, not all of these head positions can be carried out easily, which will cause more difficulties for using the INSs. The present findings confirmed that with inferior turbinate expansion, it is not very useful to change the head tilt angle to improve the particle escaping ratio.

Unlike the previous study on particle deposition inside a healthy nasal cavity (laminar flow assumption),<sup>(15–17)</sup> a turbulent  $k - \omega$  model with SST option was used for the current simulation. Generally, the existence of turbulence changes local flow pattern greatly and helps to enhance local particle transportation and deposition. Computational turbulent flow is much more of an art than that in laminar flow modeling, and remains as a challenging and controversial problem.<sup>(24–26)</sup> The laminar, transition, and turbulence regions are not well understood in such a complex nasal cavity, especially for noses with different nasal physiological symptoms. For the current nasal obstruction models with inferior turbinate hypertrophy, the cross-section along the nasal cavity is decreased, which raises the airway structure complexities inside, increases local flow intensity, and is prone to induce local turbulence more easily. Thus, it is reasonable and necessary to implement a turbulent flow model to represent the relationship between the morphological variations in nasal cavity and their influence on respiratory air flow and particle deposition accurately.

One assumption in the computation is that the flow rate is unchanged among the cases presented here. This is because the person suffering from nasal obstruction would still desire to receive the same amount of oxygen (and flow rate) during the breathing process, but at the expense of higher breathing force and higher pressure drop. The usage of the mouth to breath air in order to compensate for the nasal blockage was not considered in this study, as that could lead to an extremely complex, computationally prohibitive numerical model. Such studies can be undertaken following improvements in the available computing resources.

The “discrete phase model” is applicable for studying the movement of the drug particles in the nasal cavity, as the total volume flow rate of the drug particles is very small relative to the volume flow rate of air during nasal drug delivery. The particles are reasonably assumed to be inert, as the electrostatic forces acting among them are negligible compared to the physical forces of gravity and drag. Furthermore, the simulated dispersed particles were assumed to have a density equal to that of water ( $1000 \text{ kg/m}^3$ ). This can be explained by the fact that most of the nasal spray solutions are aqueous solutions of the drug,<sup>(35,36)</sup> which are relatively simple to develop and manufacture compared to solid dosage forms. Thus, for the particle boundary conditions along the nasal wall, a complete “trap” condition was also acceptable once they hit the nasal mucosa.

One shortcoming in this study is that the model of enlarging inferior turbinate was made homogeneously and artificially throughout the entire turbinate on both sides. This kind of artificially change in the inferior turbinate was also previously implemented with its partial reduction<sup>(37)</sup> and complete removal on one side.<sup>(38,39)</sup> These studies reported greatly disturbed intranasal air flow pattern and air conditioning with sinus surgery, which helped to understand and interpret *in vivo* measured data; however, their effects on particle deposition were not attempted. For the current two states of inferior turbinate expansion on both sides, the nu-

merical results provide a relatively fast and straightforward way to investigate their effects on the particle deposition. In the future, more histological and imaging studies are needed to have a realistic and statistical view of mucosa swelling in patients with inferior turbinate hypertrophy.

### Conclusions

In conclusion, this computational study provides qualitative and quantitative information on improved usage of intranasal medications for patients with inferior turbinate hypertrophy, which will contribute to the improvement of clinical efficacy of the drug delivery. It is noted that the patients with nasal obstruction need to ensure the presence of a middle inspiratory flow rate, when using the nasal spray device for higher escaping ratio. To insert the spray deeper with particles beyond the MCA region or a decongestive treatment to increase the MCA may be necessary in patients with moderately or severely blocked noses as the effects of the changes of nose flow rate, initial particle velocity, particle diameter, and head tilt angles for drug delivery are limited or even negligible.

### Acknowledgments

The authors acknowledge the financial support of the Academic Research Grant (T208A3103) from the Ministry of Education, Singapore. The research done under the project was approved by the relevant institutional review board.

### Author Disclosure Statement

The authors declared that no conflict of interest exists.

### References

- Bousquet J, van Cauwenberge P, Khaltaev N, Ait-Khaled N, Annesi-Maesano I, Baena-Cagnani C, Bateman E, Bonini S, Canonica GW, Carlsen KH, Demoly P, Durham SR, Enarson D, Fokkens WJ, van Wijk RG, Howarth P, Ivanova NA, Kemp JP, Klossek JM, Lockey RF, Lund V, Mackay I, Malling HJ, Meltzer EO, Mygind N, Okunda M, Pawankar R, Price D, Scadding GK, Simons FER, Szczeklik A, Valovirta E, Vignola AM, Wang DY, Warner JO, and Weiss KB: Allergic rhinitis and its impact on asthma (ARIA) (ARIA Workshop Report). *J Allergy Clin Immunol*. 2001;108:S147-S334.
- Fokkens W, Lund V, and Mullol J: European position paper on rhinosinusitis and nasal polyps. *Rhinology*. 2007;20 (Suppl):1-136.
- Senocak D, Senocak M, and Bozan S: Sinonasal distribution of topically applied particles: computerized tomographic detection and the effects of topical decongestion. *Otolaryngol Head Neck Surg*. 2005;133:944-948.
- Homer JJ, Maughan J, and Burniston M: A quantitative analysis of the intranasal delivery of topical nasal drugs to the middle meatus: spray versus drop administration. *J Laryngol Otol*. 2002;116:10-13.
- Newman SP, Steed KP, Hooper G, and Brickwell J: Scintigraphic assessment of the oropharyngeal and nasal depositions of fufasungine from a pressurized inhaler and from a novel pump spray device. *J Pharm Pharmacol*. 1995;47:818-821.
- Dowley AC, and Homer JJ: The effect of inferior turbinate hypertrophy on nasal spray distribution to the middle meatus. *Clin Otolaryngol Allied Sci*. 2001;26:488-490.
- Merkus P, Ebbens FA, Muller B, and Fokkens WJ: The "best method" of topical nasal drug delivery: comparison of seven techniques. *Rhinology*. 2005;43:102-107.
- Grant O, Bailie N, Watterson J, Cole J, Gallagher G, and Hanna B: Numerical model of a nasal septal perforation. *Medinfo*. 2004;11:1352-1356.
- Wexler D, Segal R, and Kimbell J: Aerodynamic effects of inferior turbinate reduction, computational fluid dynamics simulation. *Arch Otolaryngol Head Neck Surg*. 2005;131: 1102-1107.
- Lindemann J, Brambs HJ, Keck T, Wiesmiller KM, Rettinger G, and Pless D: Numerical simulation of intranasal airflow after radical sinus surgery. *Am J Otolaryngol*. 2005;26:175-180.
- Zhao K, Pribitkin EA, Cowart BJ, Rosen D, Scherer PW, and Dalton P: Numerical modeling of nasal obstruction and endoscopic surgical intervention: outcome to airflow and olfaction. *Am J Rhinol*. 2006;20:308-316.
- Hörschler I, Meinke M, and Schröder W: Numerical simulation of the flow field in a model of the nasal cavity. *Comput Fluid*. 2003;32:39-45.
- Pless D, Keck T, Wiesmiller K, Rettinger G, Aschoff AJ, Fleiter TR, and Lindemann J: Numerical simulation of air temperature and airflow patterns in the human nose during expiration. *Clin Otolaryngol*. 2004;29:642-647.
- Weinhold I, and Mlynski G: Numerical simulation of airflow in the human nose. *Eur Arch Otorhinolaryngol*. 2004;261: 452-455.
- Kimbell JS, Segal RA, Asgharian B, Wong BA, Schroeter JD, Southall JP, Dickens CJ, Brace G, and Miller FJ: Characterization of deposition from nasal spray devices using a computational fluid dynamics model of the human nasal passages. *J Aerosol Med*. 2007;20:59-74.
- Inthavong K, Tian ZF, Tu JY, and Yang W: Optimising nasal spray parameters for efficient drug delivery using CFD. *Comput Biol Med*. 2008;38:713-726.
- Shi H, Kleinstreuer C, and Zhang Z: Laminar airflow and nanoparticle or vapor deposition in a human nasal cavity model. *J Biomech Eng*. 2006;128:697-706.
- Lee HP, Poh HJ, Chong FH, and Wang DY: Changes of airflow pattern in inferior turbinate hypertrophy—a computational fluid dynamics model. *Am J Rhinol*. 2009;23:153-158.
- Wang DY, Raza MT, Goh DYT, Lee BW, and Chan YH: Acoustic rhinometry in nasal allergen challenge study: which dimensional measures are meaningful? *Clin Exp Allergy*. 2004;34:1093-1098.
- Huang ZL, Wang DY, Zhang PC, and Yeoh KY: Evaluation of nasal cavity by acoustic rhinometry in the ethnic groups, Chinese, Malay and Indian. *Acta Otolaryngol*. 2001;121:844-848.
- Huang ZL, Ong KL, Goh SY, Liew HL, Yeoh KH, and Wang DY: Assessment of nasal cycle by acoustic rhinometry and rhinomanometry. *Otolaryngol Head Neck Surg*. 2003;128: 510-516.
- Chen XB, Lee HP, Chong VFH, and Wang DY: Impact of inferior turbinate hypertrophy on the aerodynamic pattern and physiological functions of the turbulent airflow—a CFD simulation model. *Rhinology*. 2010;48:163-168.
- Eccles R: Nasal airflow in health and disease. *Acta Otolaryngol*. 2000;120:580-595.
- Liu Y, Edgar AM, Gu JJ, and Matthew RJ: Numerical simulation of aerosol deposition in a 3-D human nasal cavity

- using RANS, RANS/EIM, and LES. *J Aerosol Sci.* 2007;38:683–700.
25. Xi JX, and Longest PW: Numerical predictions of sub-micrometer aerosol deposition in the nasal cavity using a novel drift flux approach. *Int J Heat Mass Transfer.* 2008;51:5562–5577.
  26. Inthavong K, Tian ZF, Li HF, Tu JY, Yang W, Xue CL, and Li CG: A numerical study of spray particle deposition in a human nasal cavity. *Aerosol Sci Technol.* 2006;40:1034–1045.
  27. Jin Y, Atul K, and Martin B: *Dynamic Modeling and Simulation for Nasal Drug Delivery, Business Briefings: Medical Devices Manufacturing & Technology.* Healthcare Team, Fluent Europe Ltd, Sheffield; pp.1–4, 2004.
  28. Pattle RE: The retention of gases and particles in the human nose. In CN Davies (ed). *Inhaled Particles and Vapours.* Pergamon Press, Oxford; pp. 302–309, 1961.
  29. Hounam RF, Black A, and Walsh M: Deposition of aerosol particles in the nasopharyngeal region of the human respiratory tract. *J Aerosol Sci.* 1971;2:341–352.
  30. Cheng YS, Holmes TD, Gao J, Guilmette RA, Li S, Surakitbanharn Y, and Rowlings C: Characterization of nasal spray pumps and deposition pattern in a replica of the human nasal airway. *J Aerosol Med.* 2001;14:267–280.
  31. Tian L, and Ahmadi G: Particle deposition in turbulent duct flows—comparisons of different model predictions. *J Aerosol Sci.* 2007;38:377–397.
  32. Newman SP, Pitcairn GR, and Dalby RN: Drug delivery to the nasal cavity: *in vitro* and *in vivo* assessment. *Crit Rev Ther Drug Carrier Syst.* 2004;21:21–66.
  33. Shanley KT, Zamankhan P, Ahmadi G, Hopke PK, and Cheng YS: Numerical simulations investigating the regional and overall deposition efficiency of the human nasal cavity. *Inhal Toxicol.* 2008;20:1093–1100.
  34. Schroeter JD, Kimbell JS, and Asgharian B: Analysis of particle deposition in the turbinate and olfactory regions using a human nasal computational fluid dynamics model. *J Aerosol Med.* 2006;19:301–313.
  35. Homer JJ, and Raine CH: An endoscopic photographic comparison of nasal drug delivery by aqueous spray. *Clin Otolaryngol Allied Sci.* 1998;23:560–563.
  36. Bateman ND, Whymark AD, Clifton NJ, and Woolford TJ: A study of intranasal distribution of azelastine hydrochloride aqueous nasal spray with different spray techniques. *Clin Otolaryngol Allied Sci.* 2002;27:327–330.
  37. Wexler D, Segal R, and Kimbell J: Aerodynamic effects of inferior turbinate reduction: computational fluid dynamics simulation. *Arch Otolaryngol Head Neck Surg.* 2005;131:1102–1107.
  38. Lindemann J, Brambs HJ, Keck T, Wiesmiller KM, Rettinger G, and Pless D: Numerical simulation of intranasal airflow after radical sinus surgery. *Am J Otolaryngol.* 2005;26:175–180.
  39. Lindemann J, Keck T, Wiesmiller KM, Rettinger G, Brambs HJ, and Pless D: Numerical simulation of intranasal air flow and temperature after resection of the turbinates. *Rhinology.* 2005;43:24–28.

Received on July 6, 2009  
in final form, January 24, 2010

Reviewed by:  
Julia Kimbell  
Edgar Matida

Address correspondence to:  
De Yun Wang, M.D., Ph.D.  
Department of Otolaryngology  
Yong Loo Lin School of Medicine  
National University of Singapore  
5 Lower Kent Ridge Road  
Singapore 119260

E-mail: entwdy@nus.edu.sg